Adsorption of Gases in Metal Organic Materials: Comparison of Simulations and Experiments

Giovanni Garberoglio,[†] Anastasios I. Skoulidas,[†,§] and J. Karl Johnson*[,†,‡]

National Energy Technology Laboratory, U.S. Department of Energy, Pittsburgh, Pennsylvania 15236, Department of Chemical Engineering, University of Pittsburgh, Pittsburgh, Pennsylvania 15261

Received: February 23, 2005; In Final Form: May 19, 2005

Molecular simulations using standard force fields have been carried out to model the adsorption of various light gases on a number of different metal organic framework-type materials. The results have been compared with the available experimental data to test the validity of the model potentials. We observe good agreement between simulations and experiments for a number of different cases and very poor agreement in other cases. Possible reasons for the discrepancy in simulated and measured isotherms are discussed. We predict hydrogen adsorption isotherms at 77 and 298 K in a number of different metal organic framework materials. The importance of quantum diffraction effects and framework charges on the adsorption of hydrogen at 77 K is discussed. Our calculations indicate that at room temperature none of the materials that we have tested is able to meet the requirements for on-board hydrogen storage for fuel cell vehicles. We have calculated the volume available in a given sorbent at a specified adsorption energy (density of states). We discuss how this density of states can be used to assess the effectiveness of a sorbent material for hydrogen storage.

I. Introduction

The recent development of fundamentally new classes of nanoporous materials based on metal organic structures has been a significant development in the field of gas storage.[1,2] Microporous metal organic frameworks (MOF), such as the so-called isoreticular metal organic frameworks (IRMOFs),[2] microporous metal organic materials (MMOMs),[3] and related materials, are promising candidates for gas storage applications because they can be synthesized in high purity, high crystallinity, potentially large quantities, and at low cost. Perhaps most importantly, MOFs can have an almost endless variety of structures and functional groups, leading to the possibility of rational design of sorbent materials tailored for specific applications.[4]

MOF-like materials have been proposed as promising candidates for storing both methane and hydrogen. On-board methane storage by adsorption is important as an alternative to compressed natural gas storage for natural-gas-powered vehicles, and several different MOFs have been evaluated for their ability to adsorb methane.[1,5−7] It has been shown that some of these materials can hold significant amounts of CH_4, on both a volumetric and a gravimetric basis.[1,5−7]

The lack of viable on-board storage technologies for H_2 is a critical roadblock to the commercial success of fuel cell vehicles. The U.S. Department of Energy (DOE) has established a series of hydrogen storage targets for automotive applications.[8] These targets include gravimetric and volumetric densities, refueling rate, system cost, cycle life, and so forth. Gravimetric and volumetric targets are geared toward providing a driving range of about 500 km between refuelings without sacrificing storage or passenger space. The 2010 goals for system gravimetric and volumetric densities are 6 wt % and 45 kg H_2 m^{-3}; the ultimate 2015 targets are more demanding at 9 wt % and 81 kg H_2 m^{-3}.[8] It should be stressed that the system density target includes all needed hardware for fuel storage, so that the amount of H_2 on a sorbent material must be significantly higher than 6 wt % to meet the DOE 2010 target.

Single-walled carbon nanotubes (SWNTs) have been promoted as sorbents for H_2 storage, thanks to several reports in the literature of very large H_2 storage capacities.[9−11] However, other reports of hydrogen adsorption on these materials have been much more modest.[12,13] There is currently a controversy in the literature about the true H_2 storage capacity of these materials and the storage mechanism.[14,15] The disparate experimental results for H_2 adsorption on SWNTs is due in part to the lack of high-purity, crystalline SWNT samples.

Microporous MOFs have several distinct advantages over carbon nanotubes as potential hydrogen storage materials. In addition to the purity and cost advantages mentioned above, the pore dimensions and pore topology can be controlled to a high degree by judiciously choosing a combination of metal atoms and organic linker molecules. MOFs can be engineered to have a high skeletal density but constructed from relatively light elements. A high skeletal density means that no large voids or mesopores, which would take volume without providing adsorption sites, are present in the material. A material with high skeletal density is key to achieving a high volumetric density of adsorbed gas. The light elements in the framework are required to obtain a high gravimetric density.

Rosi et al.[4] first proposed H_2 storage in MOFs; they measured hydrogen adsorption by gravimetric methods at both 78 and 298 K in IRMOF-1. The highest pressures investigated were about 0.75 bar at 78 K, with a reported uptake of 4.5 wt % and 20 bar at 298 K, which gave about 1 wt %. They claimed that the organic linkers are of primary importance in determining H_2 uptake. They state that IRMOF-6 and IRMOF-8, which have

* Author to whom correspondence should be addressed. E-mail: karlj@pitt.edu.
† National Energy Technology Laboratory, U.S. Department of Energy.
‡ Department of Chemical Engineering, University of Pittsburgh.
§ Present address: ExxonMobil Research and Engineering, 3225 Gallows Rd., Fairfax, VA 22037.

10.1021/jp050948l CCC: $30.25
Published on Web 06/21/2005

larger organic linkers than those of IRMOF-1, adsorb 2 and 4 times the amount of H_2 in IRMOF-1 at 298 K and 10 bar, respectively.[4] While these values are far short of the DOE targets, they are larger than adsorption reported for typical activated carbons and some reports of hydrogen storage on SWNTs.

Dybtsev and co-workers have reported adsorption of H_2 and several other simple gases in a manganese-formate-based metal organic material.[16] They reported adsorption isotherms up to 1 atm at 78 and 195 K, with a maximum uptake of 0.9 wt %.

Pan et al. have synthesized a new copper-based microporous metal coordination material that has substantially smaller pores than those of many other materials.[3] They measured hydrogen uptake at room temperature up to a pressure of nearly 48 atm, finding adsorption of about 1 wt %.

Rowsell and co-workers reported H_2 uptake in five different MOF materials.[17] They measured adsorption and desorption isotherms with both gravimetric and volumetric methods at 77 K and pressures up to 1 atm. The largest uptake that they observed was about 1.5 wt %.

None of the metal organic materials have yet been able to achieve very high uptake of H_2, although much progress has been made in synthesizing and evaluating different MOFs. There are, however, indications that H_2 adsorption could be substantially increased if the metal organic material was tailored for H_2 storage.[17] Molecular simulations can be a powerful tool for identifying molecular-level adsorption phenomena and in helping to design sorbents for gas storage. However, for molecular simulations to have predictive value, the potential models used in the simulations must first be validated against experimental data.

The first reported simulations of gas adsorption in MOF-like materials of which we are aware were performed by Kawakami and co-workers.[18] They studied adsorption of N_2, CO_2, Ar, H_2, and O_2 on a zinc-based material, the so-called Zn(BDC). They used ab initio methods to compute charge densities on the sorbent framework materials and for adsorbate molecules. They then used Monte Carlo simulations to compute adsorption of light gases at pressures up to 1 atm. In comparing framework charges computed from three different methods, they found that the values of the charges made a substantial difference for the saturation loading of CO_2. They also compared their simulation results with experimental data for N_2 and CO_2 adsorption from the literature.[19] The amounts adsorbed as predicted from simulations were from 1.7 to 3 times larger than those measured experimentally. Kawakami et al. attribute the difference between simulation and experiment to the presence of defects in the experimental materials; they assume that the model potentials are accurate.

Molecular simulations coupled with low-pressure Ar adsorption experiments have been used to characterize the sorptive properties of the Cu−BTC MOF at 87.3 K.[20] Vishnyakov and co-workers used four different potential models to represent the Ar−Ar and Ar−MOF interactions. Two of the potential models gave good quantitative agreement with the experimental data, and two others overestimated the amount adsorbed.[20] In all of their simulations, they used the potential parameters from the UFF parametrization.[21] Note, however, that they used the wrong potential parameters for the Cu atoms, apparently using the UFF parameters for Ni rather than Cu.

Skoulidas reported the first self- and transport diffusivities for any gas in a microporous metal organic material.[22] He computed diffusivities in Cu−BTC as a function of loading at 298 K. He also computed the activation energies as a function of loading. The diffusivities of Ar in Cu−BTC were found to be quite similar to those in zeolites. Skoulidas used the UFF potential for Ar−framework interactions, similar to the work of Vishnyakov et al. Skoulidas and Sholl have recently presented an extensive set of calculations for the transport diffusivities of a number of different small molecules in IRMOF-1, MOF-2, MOF-3, and Cu−BTC.[23]

Snurr and co-workers have recently published two computational studies of adsorption in MOF and MOF-like materials.[6,7] In one study, they used the standard DREIDING force field[24] to account for the solid−fluid interaction potentials between adsorbates and either bipyridine molecular squares or IRMOF-1. They modeled the adsorption of C_5-C_7 normal alkanes, cyclohexane, and benzene in crystalline bipyridine molecular squares. They also computed adsorption isotherms for the C_5-C_7 normal alkanes in IRMOF-1. The self-diffusion coefficients for methane and the C_5-C_7 *n*-alkanes were computed for low loadings in both crystalline molecular squares and IRMOF-1. The values of the self-diffusion coefficients were on the order of 10^{-9} m^2 s^{-1} for the *n*-alkanes and an order of magnitude faster for methane in either of the solids.[6] Additional simulations were carried out for randomly packed molecular squares. The randomly packed structures had some larger pores and therefore showed higher adsorption at high pressures but lower adsorption at low pressures. For benzene adsorbed in crystalline molecular squares, Snurr and co-workers compared the effects of including charge interactions between the molecular square framework atoms and the quadrupole charges on benzene. The charges on the solid atoms were computed from a Mulliken charge population from a B3LYP density functional calculation. It should be noted that the Mulliken charges are quite sensitive to the size of the basis set used in the ab initio calculation and are therefore not recommended for use in computing charges for interatomic potentials. The inclusion of charges on the framework atoms did not change the qualitative adsorption behavior of benzene in crystalline molecular squares but did shift the isotherm about 3 orders of magnitude lower in pressure. No comparison with experiments was made in this paper.

Snurr and co-workers have also used molecular modeling to investigate CH_4 adsorption in a number of different MOFs.[7] They have compared with simulations for methane adsorption on a variety of other materials as well, including zeolites, MCM-41, and single-walled carbon nanotubes. They found excellent agreement between simulations and experimental data for CH_4 adsorption on IRMOF-1 and IRMOF-6 at room temperature and pressures up to 40 bar. They used both UFF[21] and DREIDING[24] force fields and found that both gave very similar results. On the basis of the good agreement between simulation and experiments, they assumed that the adsorption properties of gases in new materials could be predicted to adequate accuracy using these standard force fields, allowing for the computational design of new sorbents. They evaluated three hypothetical MOFs that have yet to be synthesized, predicting that one of these materials will have a capacity much larger than any previously known material.[7]

Taken at face value, the results of the work of Snurr and co-workers indicate that molecular simulations should be able to predict the adsorption of various gases in arbitrary MOF-like materials with reasonable accuracy. In this paper, we show that it is not always possible to achieve good agreement between simulations and experiments for different gases in MOF-like materials.

Sagara et al.[25] have used ab initio calculations to approximate the binding energy of H_2 to IRMOF-1. They used second-order

TABLE 1: Lennard-Jones Potential Parameters for the Adsorbate Species Used in This Work

adsorbate	ϵ/k_B (K)	σ (Å)
He[28]	10.22	2.28
Ar[28]	119.8	3.4
methane[29]	148.2	3.812
H_2 (Buch)[30]	34.2	2.96
H_2 (Darkrim and Levesque)[26]	36.7	2.958

Møller−Plesset perturbation theory (MP2) coupled with extrapolation to the complete basis set limit to compute the binding of H_2 on molecules representative of the IRMOF-1 framework moieties. They also developed an ad hoc interatomic potential for H_2 interacting with the IRMOF-1. They computed effective framework atomic charges from density functional calculations, coupled with a point-charge representation of the quadrupole moment on H_2. The exact form of the H_2-H_2 potential was not given; the authors state that a repulsive core was used for H_2-H_2 interactions to "prevent clumping of the H_2 molecules". The authors apparently did not check the accuracy of their potential against bulk-phase data for H_2. The results from their calculations are very similar to our results, presented later in this paper, despite the fact that the potentials used are different.

In this work, we compute adsorption isotherms using standard potentials from the literature for several different gases in a number of different materials and compare our simulations with available experimental data. We find a good agreement in some cases and very large discrepancies in other cases. We discuss the importance of quantum diffraction effects on adsorption of hydrogen at cryogenic temperatures and find that classical simulations overestimate the amount adsorbed by 10−15%. We have examined the importance of framework charges on hydrogen uptake, using a model for H_2 that includes the quadrupole moment.[26] We found that electrostatic charges on the framework atoms substantially increase the amount adsorbed at 77 K and low pressures but have a marginal effect at high pressures. Charges do not appreciably increase adsorption at 298 K.

II. Computational Details

We have used the UFF[21] and DREIDING[24] force fields for the framework atoms. The adsorbent framework has been treated as a rigid structure at all temperatures, with atom positions obtained by X-ray scattering experiments.

The fluid−fluid potential parameters used in this work are reported in Table 1. We have used the Lorentz−Berthelot mixing rules[27] to calculate the solid−fluid Lennard-Jones (LJ) parameters. The gas molecules are described as spherically symmetric particles, with the exception of the hydrogen potential of Darkrim and Levesque (DL),[26] which treats hydrogen as a rigid, diatomic molecule, with the H−H distance fixed at 0.74 Å. This potential consists of a LJ core placed at the center of mass of the molecule, point charges of magnitude $q = 0.468|e|$ at the position of the two protons, and a charge of magnitude $-2q$ at the center of mass.

In the case of hydrogen adsorption, we have tested possible improvements on the UFF/DREIDING force fields by using the DL potential together with charges calculated from the Gaussian03[31] ab initio package using the natural bond order analysis.[32] Our framework charges are fairly similar to those reported by Sagara et al.[25] The value of the electrostatic potential at any given point generated by the framework charges was calculated by adding successive concentric layers in the supercell until convergence was reached.

TABLE 2: Unit Cell Masses, Volumes, and Free Volumes for the Materials Studied in This Work

material	mass (g per mol unit cell)	unit cell volume (Å^3)	free volume (Å^3)	V_{free}/V_{cell} (%)
MOF-2	989.6	1261.03	876.42	69.5
MOF-3	753.6	844.9	610.02	72.2
IRMOF-1 (MOF-5)	6156.8	16913.24	11595.4	68.56
IRMOF-6	6780.8	17257.72	9789.5	56.73
IRMOF-8	7356.8	27247.80	20177.25	74.05
IRMOF-14	9132.8	40640.17	31657.69	77.9
Cu−BTC	9675.2	18280.82	10743.80	58.77
manganese formate	1737.3	1788.56	437.12	24.44
Cu-MMOM	2598	2663.49	362.09	13.6

We have used the standard grand canonical Monte Carlo (GCMC) method[27,33] to simulate adsorption isotherms. The probability of attempting molecule creation and deletion was set to 0.3. The simulation data for high-pressure hydrogen have been corrected for nonideal behavior by using an equation of state.[34]

Quantum effects are important for hydrogen at low temperature. We have used the path integral formalism,[33,35] adapted to the GCMC ensemble,[27,33,36] to account for quantum effects in a number of the hydrogen simulations. We have used a Trotter number of 30 beads per molecule in our simulations. Quantum mechanical effects result in lower adsorption compared with that of classical systems.

The quantity that is experimentally measurable is the excess adsorption, which is the amount of adsorbate in excess of that of the bulk fluid at the system temperature and pressure in the available (free) volume. We have calculated the interaction of the adsorbent with helium to estimate the free volume, V_{free}, because helium is often used in experiments to evaluate V_{free}. The value of V_{free} was taken as the volume with a He−framework potential of less than 1000 K. We have tried other values of the potential cutoff and have found that V_{free} is not very sensitive to the potential cutoff. The free volumes for each of the MOFs studied in this work are reported in Table 2.

The excess adsorption ratio, in milligrams of adsorbate per gram of sorbent, was computed from

$$R_{ex} = 1000\frac{m(N_{ads} - \rho_b V_{free})}{M} \quad (1)$$

where m is the molecular weight of the adsorbate molecule, N_{ads} is the total number of molecules adsorbed in a unit cell, ρ_b is the bulk gas density, and M is the mass of a unit cell of the adsorbent. The excess weight percent adsorbed can be computed from

$$\text{wt \%} = \frac{100R_{ex}}{1000 + R_{ex}} \quad (2)$$

III. Results and Discussion

A. Comparison with Experimental Data. The agreement between the simulations, with either the UFF or the DREIDING force field, and the experiments for five of nine of the systems studied is fairly good. One can see in Figures 1 and 2 that the results obtained with the two force fields in the case of methane in Cu−BTC and hydrogen in the manganese-formate material are both able to capture the trend observed in the experiments. Given that results from calculations with the UFF and DREIDING potentials are very similar, we have used the UFF force field in all of the other simulations reported here.

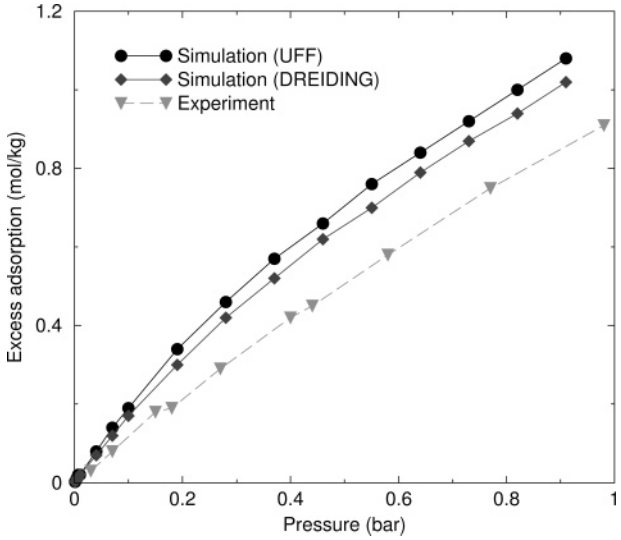

Figure 1. Adsorption of methane in Cu−BTC at 295 K. Circles and diamonds are simulation data with the UFF and DREIDING force fields, respectively. Triangles are experimental results from Wang et al.[37]

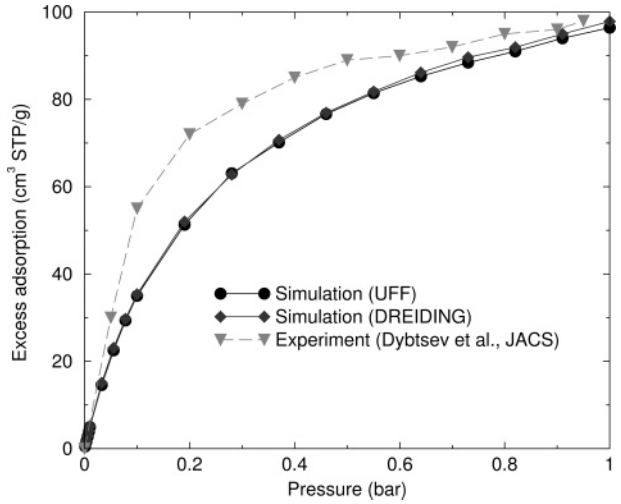

Figure 2. Adsorption of hydrogen in manganese formate at 78 K. Circles and diamonds are simulation results with the UFF and DREIDING force fields, respectively. Triangles are experimental data from Dybtsev et al.[16]

Simulations for methane in Cu−BTC (Figure 1) are in fairly good agreement with the experimental data of Wang et al.,[37] with the simulation data overestimating the experimental data only by about 10%. Our simulations for H_2 in manganese formate at 78 K compare well with the experimental data of Dybtsev et al.[16] (Figure 2). However, we note that the simulations systematically underpredict the experimental data. This is the opposite of what would be expected if the material had blocked pores or crystal defects closing off some of the adsorption sites. The simulations in Figure 2 do not include quantum corrections, which would lower the simulation data further, as discussed below. In the case of argon, we see from Figure 3 that the simulation agrees very well with the experimental data for adsorption on the Cu−BTC material[20] in the low-pressure region (up to a few millibars) and tends to overestimate the amount adsorbed at high pressures by almost 30%.

We have computed adsorption isotherms for H_2 in several of the IRMOFs and have compared the simulation data with the experimental results by Rosi et al.[4] and Rowsell et al.[17] Note that the experimental isotherm for the adsorption on IRMOF-1

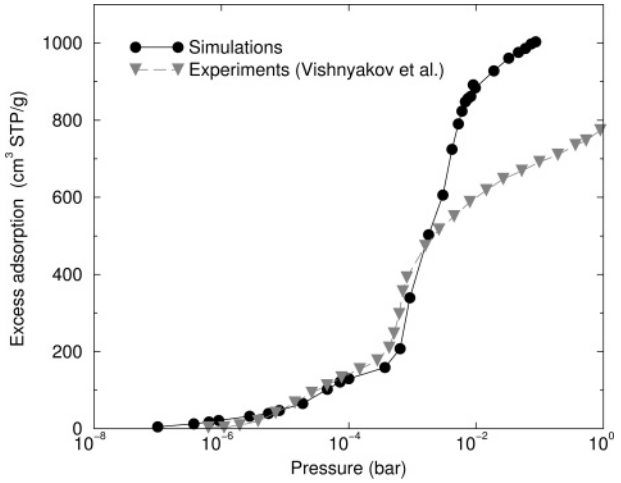

Figure 3. Adsorption of Ar in Cu−BTC. Triangles are experimental results from Vishnyakov et al.[20] Simulation data are shown as circles. The amount adsorbed is here reported in cubic centimeters of gas at standard temperature and pressure (STP, 273.15 K and 1 bar).

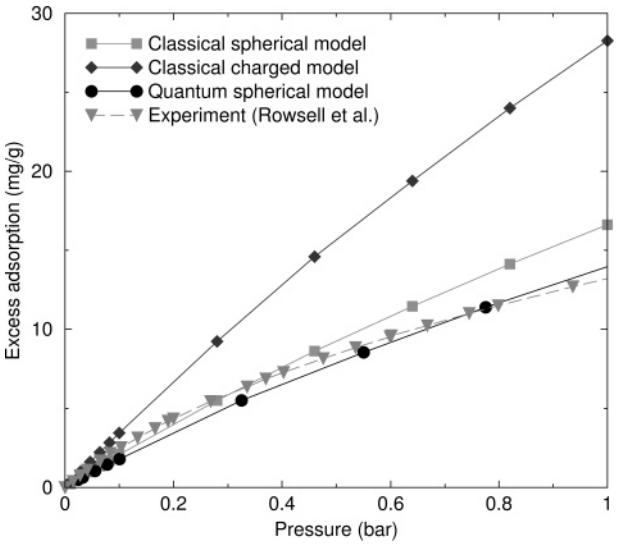

Figure 4. Adsorption of hydrogen in IRMOF-1 at 77 K. The path integral simulations with the Buch H_2 potential[30] and the UFF potential[21] for the framework atoms are plotted as circles. The squares are the classical Buch−UFF calculations. Diamonds are calculations with the Darkrim and Levesque potential.[26] The experimental data from Rowsell et al. are shown as triangles.[17]

at 77 K reported by Rowsell and co-workers[17] is qualitatively different from that reported earlier by Rosi et al.[4] on ostensibly the same material at 78 K. The earlier data display a very sudden jump in coverage at low pressures, so that the point at about 8×10^{-4} bar is reported to store 3.69 wt % H_2.[4] If we subtract the value of 3.69 wt %, then the resulting isotherm is similar to the one reported by Rowsell et al.[17]

The simulations using the classical Buch potential,[30] shown as the squares in Figure 4, are in reasonably good agreement with the experimental results; even better agreement is achieved at high loadings when quantum effects are taken into account (circles). The net effect of the explicit inclusion of quantum diffraction is to reduce the uptake with respect to a classical model. The magnitude of the reduction depends on the density of the adsorbate and is between 10% and 15% at the highest experimental pressure of 1 bar.

We have tested the importance of framework charge interactions with the H_2 quadrupole by using the DL potential, which includes a point-charge representation of the quadrupole,[26] and

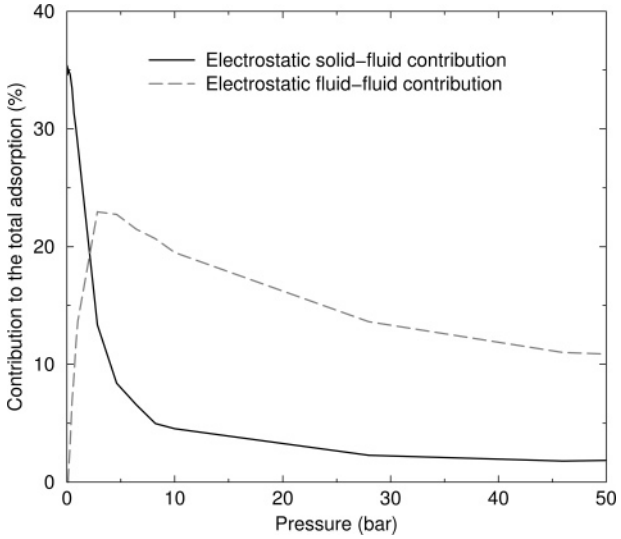

Figure 5. Effect of charges on hydrogen adsorption in IRMOF-1 at 77 K using the Darkrim and Levesque potential.[26] Solid line is the electrostatic solid−fluid contribution of eq 3. Dashed line is the electrostatic fluid−fluid contribution of eq 4.

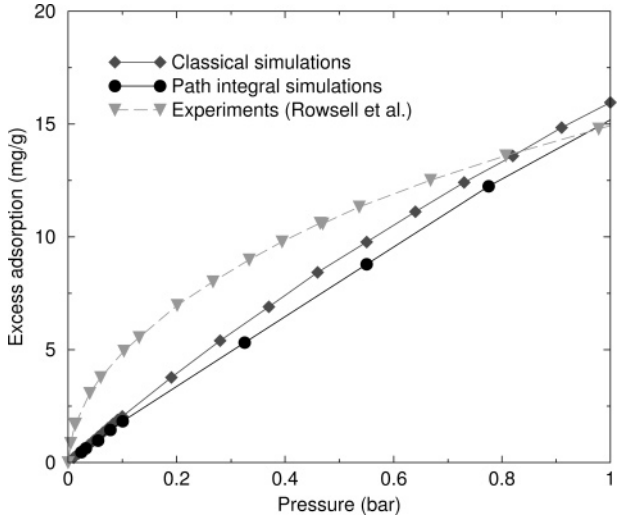

Figure 6. Adsorption of hydrogen in IRMOF-8 at 77 K. Circles are path integral simulations, and diamonds are classical simulations, both using the Buch H_2 potential[30] with UFF.[21] Experimental data from Rowsell et al.[17] are shown as triangles.

by using the charges on the IRMOF-1 framework computed from ab initio methods. The results, also shown in Figure 4 (diamonds), indicate that the amount adsorbed is dramatically enhanced by inclusion of charges. We have performed two additional calculations to separate out the role of the quadrupole−quadrupole and the quadrupole−framework charge interactions. The results from these simulations are plotted in Figure 5. We have calculated the adsorption isotherm taking into account only the LJ part of the DL potential. We identify this isotherm as $I_{LJ}(p)$, where p is the pressure. We have also calculated an adsorption isotherm using the full DL potential but switching off the framework charges, which we denote as $I_{NF}(p)$. Let $I_{DL}(p)$ be the adsorption isotherm of the full DL potential with the charged framework. We define the contribution of the solid−fluid electrostatic interaction to the adsorption isotherm relative to that of the LJ isotherm as

$$\mathrm{SF}(p) = 100\left(\frac{I_{DL}(p) - I_{NF}(p)}{I_{LJ}(p)}\right) \tag{3}$$

Likewise, the effect of the fluid−fluid quadrupolar interaction on the adsorption isotherm is defined as

$$\mathrm{FF}(p) = 100\left(\frac{I_{NF}(p) - I_{LJ}(p)}{I_{LJ}(p)}\right) \tag{4}$$

We report the functions defined in eqs 3 and 4 in Figure 5. Note that the effect of the electrostatic potentials, both solid−fluid and fluid−fluid, is always to increase the number of molecules adsorbed. The contribution of the solid−fluid electrostatics to the adsorption has a maximum at zero pressure (Henry's Law region). The low-coverage regime is enhanced by 30−40% relative to the LJ potential. The solid−fluid contribution to the adsorption decreases monotonically, contributing only a few percent at pressures >25 bar (Figure 5).

In contrast to the solid−fluid charge interactions, the contribution to the adsorption from the fluid−fluid electrostatics is zero at zero pressure, as expected, and displays a rapid increase with pressure, reaching a maximum of almost 25% relative to the LJ potential close to 5 bar. The enhancement of adsorption due to fluid−fluid electrostatics is a consequence of the fact that the quadrupole−quadrupole interaction is, on the average, attractive. As the pressure increases, the electrostatic contribution becomes less important, tending to a value around 10% at $p > 50$ bar.

Overall, the presence of electrostatic interactions results in an amount adsorbed that is about 40−45% higher than that given by the LJ core alone for $p \leq 1$ bar. The quadrupole−quadrupole terms dominate at pressures above about 5 bar, so that the effect of solid−fluid charges is actually quite small except at low pressures. The DL LJ potential is more attractive than the Buch model (Table 1), which has been shown to predict accurately the bulk hydrogen properties over a wide range of temperatures and densities.[38] We therefore conclude that inclusion of the quadrupole term in the DL potential makes the overall potential too attractive. The DL potential is therefore not suitable for simulation of hydrogen adsorbed in charged frameworks. We have tried to change the parameters in the DL potential to fit the available adsorption isotherm of H_2 in IRMOF-1, and we found that setting $\epsilon/k_B = 30$ K results in an isotherm that is similar to the one obtained by the Buch potential (and, consequently, to the available experimental data) for pressures less than 1 bar. The adsorption isotherms of the Buch and the modified DL potential start to differ for pressures greater than 4 bar, with the modified DL potential giving higher amounts adsorbed. Experimental data at 77 K and $p > 1$ bar are needed to resolve the question of which potential is more physically realistic.

Our results for the isotherm of adsorption of H_2 in IRMOF-1 are in agreement with the calculations by Sagara et al.[25] who have used an ad hoc H_2 potential model that includes a quadrupole term. The simulation results of Sagara et al. at 77 K lie between our simulations with the Buch and the DL potentials and overestimate the amount adsorbed at 1 bar by almost 20% compared with experiments.

We also find fairly good agreement between simulation and experimental results for H_2 adsorption in IRMOF-8, reported in Figure 6. However, in this case both the classical and the quantum simulations underestimate the hydrogen uptake by almost 40% for pressures under 0.6 bar. The experiments indicate a larger Henry's Law constant than the simulations, as evident by the larger initial uptake. However, the experiments and simulations are in very good agreement between 0.7 and 1

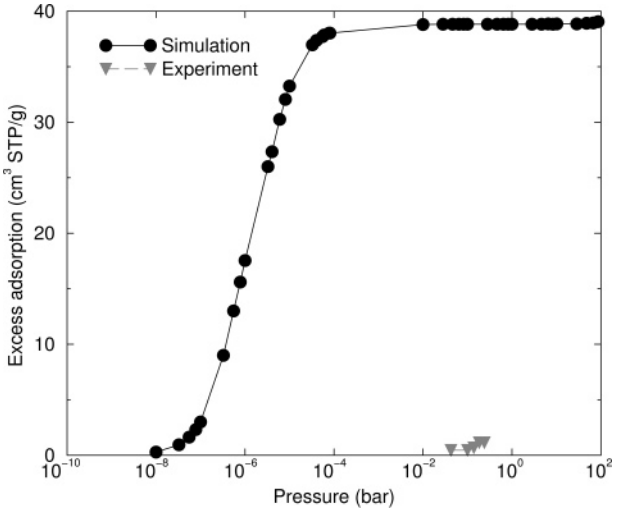

Figure 7. Adsorption of Ar in manganese formate at 78 K. Circles are simulation results. Triangles are experimental data from Dybtsev et al.[16]

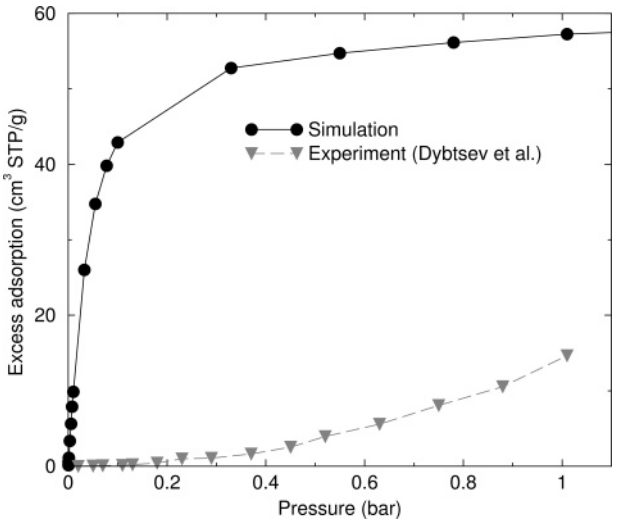

Figure 8. Adsorption of methane in manganese formate at 195 K. Circles are simulation results. Triangles are experimental data from Dybtsev et al.[16]

bar. Better agreement at low pressures may be achieved if framework charge−quadrupole interactions were included.

There are cases for which the simulations and the experiments give very different results. The first example, shown in Figure 7, is for the adsorption of argon in the manganese-formate material at 78 K.[16] The simulations predict an amount adsorbed that is about a factor of 50 larger than that observed experimentally. Moreover, the pressure at which saturation apparently occurs varies by about 3 orders of magnitude between simulation ($\simeq 10^{-4}$ bar) and experiment ($\simeq 10^{-1}$ bar). The experimental temperature in this case is below the triple point temperature of Ar ($T_{tr} = 83.8$ K). Therefore, the discrepancy may be due to the formation of bulklike argon clusters on the surface of the sorbent, which would inhibit entry of the Ar into the sorbent framework.

The adsorption of methane on manganese formate at 195 K measured experimentally[16] and computed from simulations is plotted in Figure 8. The experimental and simulation data do not agree qualitatively. The simulation data predict a classic Langmuir-type adsorption isotherm, which approaches saturation at around 1 bar. The experimental data show a modest increase in the amount adsorbed with increasing pressure, no indication

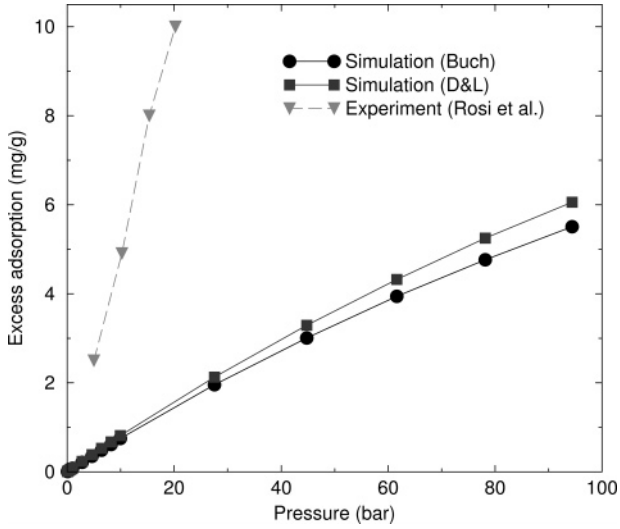

Figure 9. Adsorption of hydrogen in IRMOF-1 at 298 K. Circles and squares are simulations using the Buch[30] and Darkrim and Levesque[26] potentials, respectively. Triangles are experimental results from Rosi et al.[4]

of a plateau, and a value about a factor of 4 smaller than that predicted from simulations at ∼1 bar. The small uptake of methane is unexpected, given that Dybtsev et al. have measured large uptake of CO_2 in this same material.[16] We have computed the zero-coverage diffusivity of methane in manganese formate using the same simulation methods as in a previous publication.[22] We obtained a value of 4.66×10^{-4} cm^2 s^{-1} at 195 K, which is similar in magnitude to the diffusivity of methane in silicalite (MFI), a siliceous zeolite.[39] Therefore, slow diffusion of methane into the MOF is not likely to be a cause for the discrepancy between simulations and experiments, for which we have no viable explanation.

The discrepancy between simulations and experiments for H_2 adsorbed in IRMOF-1 at 298 K is puzzling. The good agreement between simulations and experiments for H_2 in IRMOF-1 at 77 K evident in Figure 4 leads us to expect similar agreement at 298 K. However, the experimental data[4] are about a factor of 7 greater than those predicted by simulations, as can be seen from Figure 9. Note also from Figure 9 that results from the DL potential (squares) are almost identical to the calculations from the Buch potential. Hence, framework charge−quadrupole and quadrupole−quadrupole interactions are essentially negligible at room temperature and pressures up to about 50 bar. Our simulation results are in good agreement with simulation data from Sagara et al.[25]

If the crystal structure of IRMOF-1 remains unchanged from 77 to 298 K, then there are three possibilities for explaining the differences between simulations and experiments observed in Figure 9: (1) The potentials we have used are grossly in error. If this is true, then the good agreement seen in Figure 4 is inexplicable. (2) There is some additional binding mode available at high temperature that is not evident at 77 K. Interatomic potentials are not functions of temperature, so the additional binding mode would have to be due to some chemical or physical change in the crystal or in the way in which H_2 interacts with the framework. (3) The experimental data may be in error. We cannot definitively rule out any of these possibilities at present.

Pan et al. have synthesized a new copper-based microporous metal organic material (Cu-MMOM) with very narrow one-dimensional pores.[3] The uptake of H_2 has been measured in this material at room temperature up to a pressure of 48 bar.

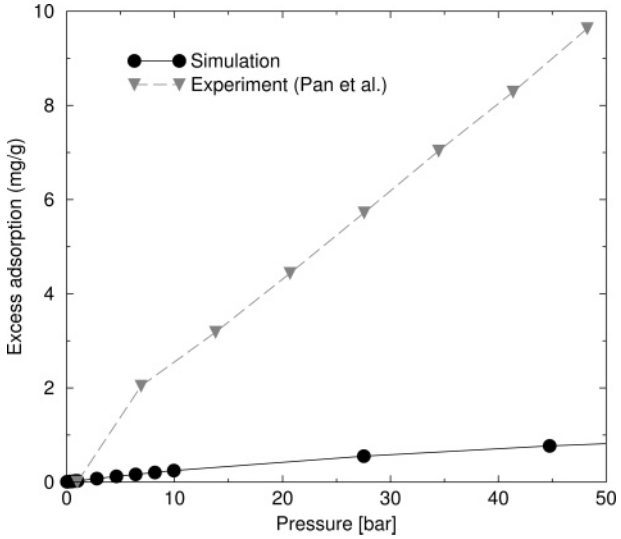

Figure 10. Adsorption of H_2 at 298 K in the copper-based material (Cu-MMOM) synthesized by Pan et al.[3] Triangles are experimental data, and circles are predictions from simulations.

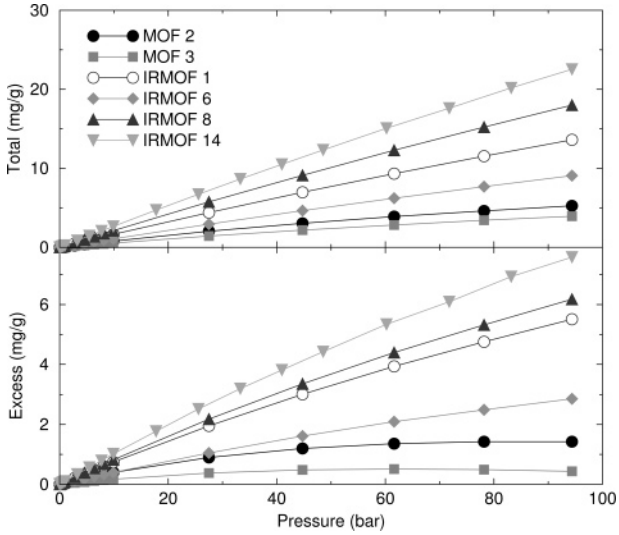

Figure 11. Hydrogen adsorption isotherms at 298 K in various MOFs predicted from simulations. The total adsorption (top) and excess adsorption (bottom) are shown.

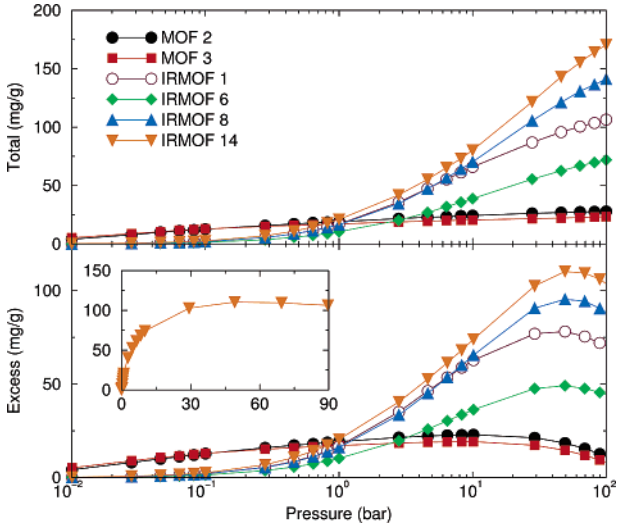

Figure 12. Hydrogen adsorption isotherms at 77 K in various MOFs predicted from simulations. These data have not been quantum-corrected and therefore overestimate the amount adsorbed.

We have simulated the adsorption isotherm in this material; the simulation and experimental data are plotted in Figure 10. The agreement between the predictions from simulations and the experimental data is very poor, with experiments giving about a factor of 10 higher adsorption than simulations.

The reason for this discrepancy may be due to the very small volume available for hydrogen in the simulation unit cell. According to our potential model, only 13.6% of the unit cell volume is available for adsorption (Table 2), which is in good agreement with the value of Pan et al. of 11.6%. Using this value together with the amount adsorbed according to the experimental isotherm at the highest pressure, one obtains a density of adsorbed hydrogen of around 119 kg m^{-3}, far in excess of the density of solid hydrogen, which is around 88 kg m^{-3}. This might indicate either an error in the isotherm measurements or an error in the calculation of the atomic coordinates from the diffraction data.

B. Prediction of Adsorption Isotherms. In this section, we present predictions for H_2 adsorption in several different MOFs at state points for which no experimental isotherms have yet been published, namely, MOF-2, MOF-3, IRMOF-6, IRMOF-8, and IRMOF-14. Adsorption isotherms at 298 and 77 K are shown in Figures 11 and 12, respectively. We have also included our calculated isotherms for IRMOF-1 in these figures for comparison. Total adsorption is reported in the top panels, with excess adsorption, which can be compared with experiments, shown in the bottom panels of Figures 11 and 12. The isotherms should be viewed as qualified predictions, since one does not always get good agreement between predicted and measured isotherms. Nevertheless, simulations are useful for examining the trends of adsorption in different materials.

The shapes of the isotherms at 298 K (Figure 11) are very similar, indicating a common mechanism for adsorption in the different materials. This is the result of nonspecific binding with the framework atoms at high temperatures, resulting in relatively weak physisorption between the H_2 molecules and the sorbent.

The material with the highest uptake over the entire pressure range at 298 K is IRMOF-14, for both total and excess adsorption. Our simulated isotherms indicate that none of the MOFs that we have tested are likely to be able to meet the DOE targets for gravimetric storage density at 298 K and pressures less than 100 bar, assuming that our simulations are accurate. The largest total uptake predicted from simulations at room temperature and 100 bar is about 23 mg g^{-1} or 2 wt %. However, if one assumes that our simulation results are a factor of 7 lower than the actual experimental isotherms, as indicated in Figure 9, then the total adsorption in IRMOF-14 could be as high as 14 wt %, which would be sufficiently high to meet the DOE target.

We note that the data in Figure 11 are not in agreement with the claims made by Rosi et al. that H_2 adsorption at room temperature and 10 bar in IRMOF-1, IRMOF-6, and IRMOF-8 is 0.5, 1, and 2 wt %, respectively.[4] The qualitative trends in the simulations and experiments are different; simulations predict that the excess adsorption is 0.16, 0.1, and 0.2 wt % for IRMOF-1, IRMOF-6, and IRMOF-8, respectively. The smaller uptake in IRMOF-6 compared with that of IRMOF-1 is due to the smaller available volume (Table 2). Full experimental isotherms over a range of pressures are needed for these three materials to resolve the differences between the simulations and the data reported by Rosi et al.

The adsorption isotherms at cryogenic conditions (Figure 12) are very different from those at room temperature. The MOF-2

and MOF-3 materials have very similar isotherms. The isotherms are relatively flat, with higher uptake at 10^{-2} bar than for any of the other materials, but having lower uptake for $p > 3$ bar. The excess mass isotherms plotted in Figure 12 (bottom) display maxima for all materials at pressures between 30 and 70 bar. A maximum in the excess adsorption isotherm is expected for any gas above its critical temperature at high enough pressures. The IRMOF materials all have isotherms of similar shape, which on the log−linear scale appear to be somewhat "S-shaped". When plotted on a linear scale, the isotherms have the usual "Langmuir shape" (inset). The maximum amount of H_2 adsorbed is achieved in the IRMOF-14 material, as was the case for the 298 K isotherm. The amount adsorbed is about an order of magnitude larger at 77 K compared with that at 298 K. The total amount adsorbed at 100 bar in IRMOF-14 is 171 mg g^{-1} or almost 15 wt %. The much smaller uptake observed for MOF-2 and MOF-3 compared with the IRMOFs can be partly explained in terms of the ratio of free volume to the crystal mass (Table 2). For MOF-2, this ratio is 0.53 cm^3 g^{-1}, while for IRMOF-14 the ratio is 2.1 cm^3 g^{-1}. Hence, there is far less volume available per weight in the MOFs than that for the IRMOFs investigated in Figures 11 and 12. We note from Figure 12 that materials that have a similar structure have isotherms that are of the same shape and similar qualitative adsorptive behavior. Quantum effects were not included in the simulation data in Figure 12 for computational efficiency. The data are therefore probably about 15% too high in the higher pressure range.

The reason for the low adsorption predicted for H_2 at room temperature in these materials is that the adsorption energies are not sufficiently large. For the free energy of adsorption to be favorable, one must have an enthalpy of adsorption large enough to overcome the entropy loss upon adsorption

$$\Delta G^{ads} = \Delta H^{ads} - T\Delta S^{ads} < 0 \qquad (5)$$

The ideal gas translational entropy of H_2 at $T = 298$ K and 100 bar is 79 J mol^{-1} K^{-1}, so that if all translational entropy were lost upon adsorption, then $T\Delta S^{ads} = -24$ kJ mol^{-1}. If only one degree of translational entropy were lost upon adsorption (as might be the case for a gas adsorbed on a smooth surface), then $T\Delta S^{ads}$ would be about −14 kJ mol^{-1}.[40] Thus, a crude estimate is that a heat of adsorption between −20 and −10 kJ mol^{-1} is needed to achieve a very high adsorption of H_2 at room temperature and moderate pressures.

The isosteric heats of adsorption, q_{st}, of H_2 in various MOFs are plotted in Figure 13. Note that the largest value of q_{st} occurs for MOF-3 and is about 8.8 kJ mol^{-1}. Assuming that $q_{st} \approx -\Delta H^{ads}$ (which is valid in the ideal gas limit[41]), we conclude that the isosteric heats in the best materials are too small by roughly a factor of 2. Note that the isosteric heats at 298 K are essentially independent of pressure, indicating that even at 100 bar the isosteric heat is close to the zero-coverage limit. In contrast, q_{st} decreases with increasing pressure at 77 K, especially for MOF-2 and MOF-3, indicating that at higher coverage not all molecules are able to occupy the most energetically favorable adsorption sites. The q_{st} values at 77 K for the IRMOFs do not decrease as dramatically as those for the MOFs. Note, however, that there is a noticeable decrease in q_{st} for IRMOF-14, for which the loading is the highest.

It may appear that the isosteric heats reported in Figure 13 are not consistent with the adsorption isotherms seen in Figures 11 and 12, since MOF-2 and MOF-3 have the highest values of q_{st} but the lowest uptake. It is evident that a large value of the isosteric heat is not sufficient to achieve high adsorption

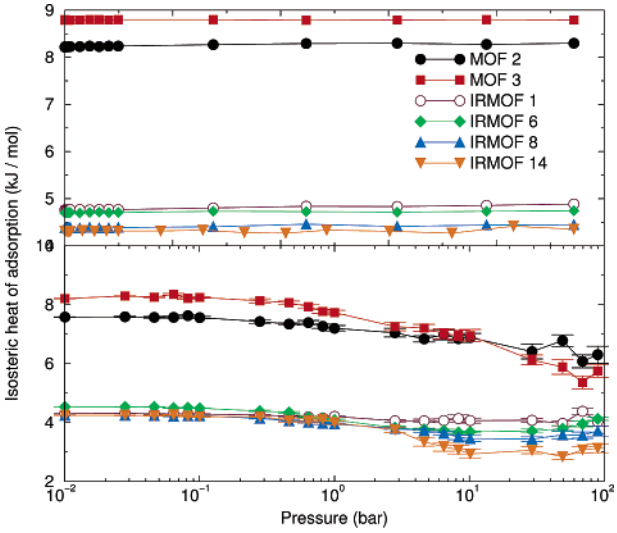

Figure 13. Isosteric heats of adsorption for H_2 adsorbed in various MOFs at 298 K (top) and 77 K computed from simulations. The error bars in the top graph are smaller than the size of the symbols.

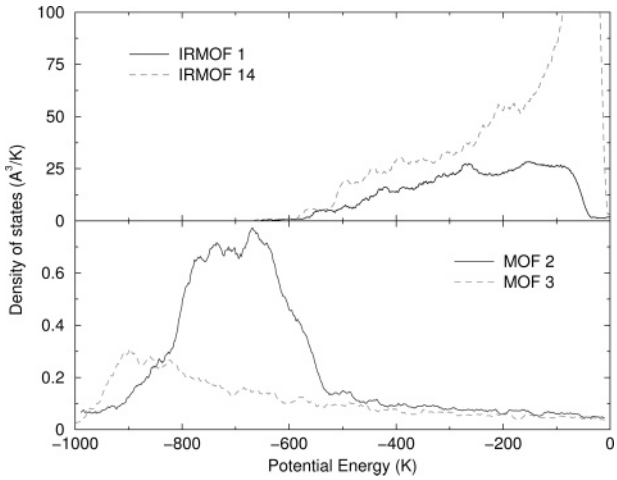

Figure 14. Volume density of states for H_2 interacting with four different MOFs.

capacity. The reason for MOF-2 and MOF-3 having lower uptake than the IRMOFs at 298 K is that the volume available for adsorption *at high heat of adsorption* is small. The amount of volume available for adsorption at a given adsorption energy can be quantified by computing the *volume density of states*. We define the density of states such that $D(E)\,dE$ is the volume of space available to an adsorbate molecule at adsorption energies between E and $E + dE$. We have computed the density of states by numerical differentiation of the volume available for adsorbate−adsorbent energies less than E. This approach is similar in spirit to the adsorption energy distribution method,[42] which has been extensively used to calculate isotherms on heterogeneous surfaces. However, the volume density of states accounts for the potential energy field in a volume rather than on a surface, as the adsorption energy distribution method does. This is important because it is not sufficient to account only for surface site adsorption in narrow pores, where the potential field may be high enough to stabilize multiple layers of sorbate molecules. The density of states for IRMOF-1 and IRMOF-14 are plotted in the upper panel, and the density of states for MOF-2 and MOF-3 are plotted in the lower panel of Figure 14. Note that the density of states for MOF-2 and MOF-3 extends to lower energies than the two IRMOFs but that the values of the density of states are about an order of magnitude

larger for IRMOF-1 and IRMOF-14 (note the change in scale between the upper and lower panel of Figure 14).

We can use the density of states as an approximate way to define an "ideal" sorbent material for hydrogen storage. We assume that adsorption takes place at some temperature T at a pressure P_2 and that desorption takes place at T and some lower pressure P_1. Now assume that the adsorption energies must lie in the range $E_2 < E < E_1$ for a sufficient quantity of H_2 to adsorb from the gas phase at pressure P_2 and desorb at a pressure P_1. The free energy of adsorption can be related to the heat of adsorption and hence to the entropy of adsorption through eq 5. Further assume that the average density of the adsorbed phase is ρ_{ads}. Then the volume per unit cell required to adsorb a given total (not excess) weight percent is

$$V_{DOS} = \frac{1}{\rho_{ads}}\left(\frac{\text{wt \%} \times M}{100 - \text{wt \%}}\right) \tag{6}$$

where wt % is the total weight percent of H_2 and M is the mass of a unit cell of the adsorbent, as in eq 1. The value of V_{DOS} is related by an integral over the density of states through the energies E_1 and E_2

$$V_{DOS}(E_2,E_1) = \int_{E_1}^{E_2} D(E)\, dE \tag{7}$$

Hence, if we define the temperature, adsorption and desorption pressures, and the weight of the sorbent material, then we can, in principle, compute the volume required to achieve a given total weight percent of gas adsorbed. As an example, we calculate the V_{DOS} needed in IRMOF-14 to store 10 wt %. We assume that wt % = 10% is needed to achieve a *system* gravimetric density of 6% (the extra 4% being needed to make up for the pressure tank and associated hardware). Using the mass of IRMOF-14, $M = 1.517 \times 10^{-23}$ kg per unit cell, in eq 6 and assuming that the density of the adsorbed phase is that of liquid H_2 (71.1 kg m^{-3}), then $V_{DOS} = 23\,700$ Å^3. The total available volume in IRMOF-14 is 31 658 Å^3 (Table 2), so this calculation indicates that 75% of the total available volume must have an adsorption energy between E_1 and E_2. The entropy argument gives an order of magnitude estimate that E should be in the range from −20 to −10 kJ mol^{-1} (−2400 to −1200 K). We note from Figure 14 that we see that none of the materials plotted have a density of states in the correct range. The adsorption energy of IRMOF-14 would need to be increased by about a factor of 5. We stress that the energies given here are just rough estimates.

IV. Conclusions

In this paper, we have presented computer simulations with standard force fields and assessed their performance in the prediction of adsorption isotherms for light gases in several different MOF-like materials. We have used a rigid model for the adsorbent structure, with the framework coordinates obtained by X-ray scattering.

The results indicate that the model is able to reproduce adsorption isotherms for Ar, CH_4, and H_2 in selected materials within 10−15% of the experimental values. However, very large discrepancies between simulations and experiments have also been noted. The most puzzling case is for adsorption of H_2 in IRMOF-1. The path integral simulation results at 77 K are in excellent agreement with experiments, whereas at room temperature the simulations underestimate the amount of adsorbed hydrogen by a factor of 7.

We have investigated the importance of framework charges on the adsorption of H_2 in IRMOF-1 as a function of temperature and pressure. Charge−quadrupole interactions enhance substantially the adsorption at 77 K and low pressures ($p < 5$ bar), but the effect is only a few percent at higher pressures (Figure 5). Charge−quadrupole interactions do not significantly change the amount adsorbed at room temperature.

We have predicted H_2 adsorption in MOF-2, MOF-3, and IRMOFs 1, 6, 8, and 14 at 77 and 298 K and pressures up to 100 bar. Assuming that the potentials that we use are accurate, we predict that none of the MOFs that we have examined are able to meet the DOE targets at room temperature. However, IRMOF-14 exhibits very high uptake at 77 K, giving a maximum excess adsorption of about 10 wt % and a total uptake of 15 wt %.

We have computed the volume density of states for several different MOFs. We present a simple energetic model for the density of states required to achieve high uptake of H_2 at room temperature. Our model indicates that none of the existing MOFs that we have tested have large density of states at low enough energies to store significant amounts of hydrogen at room temperature. The model can be used to help design new sorbent materials for H_2 storage.

Acknowledgment. We thank Channing Ahn, Bradly Bockrath, Jing Li, Christopher Matranga, David Sholl, Milton Smith, and John Vajo for helpful discussions.

References and Notes

(1) Eddaoudi, M.; Kim, J.; Rosi, N.; Vodak, D.; Wachter, J.; O'Keefe, M.; Yaghi, O. M. *Science* **2002**, *295*, 469−472.

(2) Yaghi, O. M.; Keeffe, M. O.; Ockwig, N. W.; Chae, H. K.; Eddaoudi, M.; Kim, J. *Nature* **2003**, *423*, 705−714.

(3) Pan, L.; Sander, M. B.; Huang, X. Y.; Li, J.; Smith, M.; Bittner, E.; Bockrath, B.; Johnson, J. K. *J. Am. Chem. Soc.* **2004**, *126*, 1308−1309.

(4) Rosi, N. L.; Eckert, J.; Eddaoudi, M.; Vodak, D. T.; Kim, J.; O'Keefe, M.; Yaghi, O. M. *Science* **2003**, *300*, 1127−1129.

(5) Kondo, M.; Okubo, T.; Asami, A.; Noro, S.; Yoshitomi, T.; Kitagawa, S.; Ishii, T.; Matsuzaka, H.; Seki, K. *Angew. Chem., Int. Ed.* **1999**, *38*, 140−143.

(6) Sarkisov, L.; Düren, T.; Snurr, R. Q. *Mol. Phys.* **2004**, *102*, 211−221.

(7) Düren, T.; Sarkisov, L.; Yaghi, O. M.; Snurr, R. Q. *Langmuir* **2004**, *20*, 2683−2689.

(8) *Multi-Year Research, Development and Demonstration Plan: Planned Program Activities for 2003−2010: Technical Plan*; U.S. Department of Energy; http://www.eere.energy.gov/hydrogenandfuelcells/mypp/pdfs/storage.pdf.

(9) Dillon, A. C.; Jones, K.; Bekkedahl, T. A.; Kiang, C. H.; Bethune, D. S.; Heben, M. J. *Nature* **1997**, *386*, 377−379.

(10) Liu, C.; Fan, Y. Y.; Liu, M.; Chong, H. T.; Cheng, H. M.; Dresselhaus, M. S. *Science* **1999**, *286*, 1127−1129.

(11) Dresselhaus, M. S.; Williams, K. A.; Eklund, P. C. *MRS Bull.* **1999**, *24*, 45−50.

(12) Tibbetts, G. G.; Meisner, G. P.; Olk, C. H. *Carbon* **2001**, *39*, 2291−2301.

(13) Lawrence, J.; Xu, G. *Appl. Phys. Lett.* **2004**, *84*, 918−920.

(14) Hirscher, M.; Becher, M.; Haluska, M.; von Zeppelin, F.; Chen, X. H.; Dettlaff-Weglikowska, U.; Roth, S. *J. Alloys Compd.* **2003**, *356*, 433−437.

(15) Becher, M.; Haluska, M.; Hirscher, M.; Quintel, A.; Skakalova, V.; Dettlaff-Weglikovska, U.; Chen, X.; Hulman, M.; Choi, Y.; Roth, S.; Meregalli, V.; Parrinello, M.; Ströbel, R.; Jörissen, L.; Kappes, M. M.; Fink, J.; Züttel, A.; Stepanek, I.; Bernier, P. *C. R. Phys.* **2003**, *4*, 1055−1062.

(16) Dybtsev, D. N.; Chun, H.; Yoon, S. H.; Kim, D.; Kim, K. *J. Am. Chem. Soc.* **2004**, *126*, 32−33.

(17) Rowsell, J. L.; Millward, A. R.; Park, K. S.; Yaghi, O. M. *J. Am. Chem. Soc.* **2004**, *126*, 5666−5667.

(18) Kawakami, T.; Takamizawa, S.; Kitagawa, Y.; Maruta, T.; Mori, W.; Yamaguchi, K. *Polyhedron* **2001**, *20*, 1197−1206.

(19) Li, H.; Eddaoudi, M.; Groy, T. L.; Yaghi, O. M. *J. Am. Chem. Soc.* **1998**, *120*, 8571−8572.

(20) Vishnyakov, A.; Ravikovitch, P. I.; Neimark, A. V.; Bulow, M.; Wang, Q. M. *Nano Lett.* **2003**, *3*, 713−718.

(21) Rappé, A.; Casewit, C. J.; Colwell, K. S., Goddard, W. A., III; Skiff, W. M. *J. Am. Chem. Soc.* **1992**, *114*, 10024.
(22) Skoulidas, A. I. *J. Am. Chem. Soc.* **2004**, *126*, 1356−1357.
(23) Skoulidas, A. I.; Sholl, D. S. *J. Phys. Chem. B*, in press.
(24) Mayo, S.; Olafson, B.; Goddard, W. A., III *J. Phys. Chem.* **1990**, *94*, 8897.
(25) Sagara, T.; Klassen, J.; Ganz, E. *J. Chem. Phys.* **2004**, *121*, 12543.
(26) Dakrim, F.; Levesque, D. *J. Chem. Phys.* **1998**, *109*, 4981−4984.
(27) Allen, M.; Tildesley, D. *Computer Simulation of Liquids*; Oxford University Press: Oxford, U. K., 1989.
(28) Maitland, G. C.; Rigby, M.; Smith, E. B.; Wakeham, W. A. *Intermolecular Forces: Their Origin and Determination*; Clarendon Press: Oxford, U. K., 1981.
(29) Jiang, S.; Gubbins, K. E.; Zollweg, J. A. *Mol. Phys.* **1993**, *83*, 103.
(30) Buch, V. *J. Chem. Phys.* **1994**, *100*, 7610−7629.
(31) Frisch, M. J.; Trucks, G. W.; Schlegel, H. B.; Scuseria, G. E.; Robb, M. A.; Cheeseman, J. R.; Montgomery, Jr., J. A.; Vreven, T.; Kudin, K. N.; Burant, J. C.; Millam, J. M.; Iyengar, S. S.; Tomasi, J.; Barone, V.; Mennucci, B.; Cossi, M.; Scalmani, G.; Rega, N.; Petersson, G. A.; Nakatsuji, H.; Hada, M.; Ehara, M.; Toyota, K.; Fukuda, R.; Hasegawa, J.; Ishida, M.; Nakajima, T.; Honda, Y.; Kitao, O.; Nakai, H.; Klene, M.; Li, X.; Knox, J. E.; Hratchian, H. P.; Cross, J. B.; Bakken, V.; Adamo, C.; Jaramillo, J.; Gomperts, R.; Stratmann, R. E.; Yazyev, O.; Austin, A. J.; Cammi, R.; Pomelli, C.; Ochterski, J. W.; Ayala, P. Y.; Morokuma, K.; Voth, G. A.; Salvador, P.; Dannenberg, J. J.; Zakrzewski, V. G.; Dapprich, S.; Daniels, A. D.; Strain, M. C.; Farkas, O.; Malick, D. K.; Rabuck, A. D.; Raghavachari, K.; Foresman, J. B.; Ortiz, J. V.; Cui, Q.; Baboul, A. G.; Clifford, S.; Cioslowski, J.; Stefanov, B. B.; Liu, G.; Liashenko, A.; Piskorz, P.; Komaromi, I.; Martin, R. L.; Fox, D. J.; Keith, T.; Al-Laham, M. A.; Peng, C. Y.; Nanayakkara, A.; Challacombe, M.; Gill, P. M. W.; Johnson, B.; Chen, W.; Wong, M. W.; Gonzalez, C.; Pople, J. A. *Gaussian 03*, revision C.02; Gaussian, Inc.: Wallingford, CT, 2004.
(32) Reed, A. E.; Curtiss, L. A.; Weinhold, F. *Chem. Rev.* **1988**, *88*, 899.
(33) Landau, D.; Binder, K. *A Guide to Monte Carlo Simulations in Statistical Physics*; Cambridge University Press: Cambridge, U. K., 2000.
(34) Younglove, B. A. *J. Phys. Chem. Ref. Data* **1982**, *11*(Suppl. 1), 1−349.
(35) Feynman, R. P. *Rev. Mod. Phys.* **1948**, *20*, 367−387.
(36) Wang, Q.; Johnson, J.; Broughton, J. *J. Chem. Phys.* **1997**, *108*, 5117.
(37) Wang, Q.; Shen, D. M.; Bulow, M.; Lau, M. L.; Deng, S. G.; Fitch, F. R.; Lemcoff, N. O.; Semanscin, J. *Microporous Mesoporous Mater.* **2002**, *55*, 217−230.
(38) Wang, Q.; Johnson, J.; Broughton, J. *Mol. Phys.* **1996**, *89*, 1105−1119.
(39) Skoulidas, A. I.; Sholl, D. S. *J. Phys. Chem. B* **2001**, *105*, 3151−3154.
(40) The entropy of a two-dimensional gas depends on the density. We have assumed a close-packed density of H_2 in this calculation.
(41) Myers, A.; Siperstein, F. *Colloids Surf., A* **2001**, *187−188*, 73.
(42) Rudzinski, W.; Everett, D. *Adsorption of Gases on Heterogeneous Surfaces*; Academic Press: San Diego, CA, 1992.